Microstructural investigations of carbon foams derived from modified coal-tar pitch

George Tzvetkov[a,*], Boyko Tsyntsarski[b], Konstantin Balashev[a], Tony Spassov[a]

[a]Faculty of Chemistry and Pharmacy, University of Sofia, J. Bourchier 1, 1164 Sofia, Bulgaria

[b]Institute of Organic Chemistry with Centre of Phytochemistry,
Bulgarian Academy of Sciences, Acad. G. Bonchev str., BL. 9, 1113 Sofia, Bulgaria

*Corresponding author. Fax: +3592-9625-438, Phone: +3592-8161-206.
E-mail address: george.tzvetkov@gmail.com (G. Tzvetkov)

Highlights

● The microstructure of coal-tar pitch-derived carbon foams is examined.

● Microspheres containing sp-bonded species are observed at 1000 ºC.

● Above 1000 ºC the microspheres experience transformations in a non-aromatic pathway.

● Microspheres are identical with the sp^2-sp^3 foams matrices at 2000 ºC.

● The compressive strength depends on the concentration of sp-bonded carbon atoms.

Abstract

This work reports the microstructural evaluation of carbon foams derived from coal-tar pitch precursors treated with H_2SO_4 and HNO_3 and finally annealed at 1000 ºC and 2000 ºC. Our experimental investigations combine scanning electron microscopy (SEM), transmission electron microscopy (TEM), atomic force microscopy (AFM) imaging, X-ray photoelectron spectroscopy (XPS) and micro-spot near-edge X-ray absorption fine structure (μ-NEXAFS) spectroscopy. This set of complementary techniques provides detailed structural and chemical information of the surface and the bulk of the carbon foams. The high-resolution microscopy data indicate the formation of carbonaceous amorphous microspheres (average diameters of 0.28±0.01 μm) embedded in the partially graphitized carbon foam matrix at 1000 ºC. The microspheres are enriched with sp-bonded species and their microstructural characteristics depend on the reagent (nitric *vs*. sulfuric acid) used for pitch treatment. A complete chemical transformation of the microspheres at temperatures >1000 ºC occurs and at 2000 ºC they are spectroscopically identical with the bulk material (sp^2- and sp^3-hybridised forms of carbon). The microstructure-property relationship is exemplified by the compressive strength measurements. These results allow a better description of coal-tar pitch-derived carbon foams at the atomic level, and may account for a better understanding of the processes during graphitization step.

Keywords: Carbon foam; SEM; TEM; AFM; XPS; NEXAFS

Introduction

During the last two decades carbon foam materials have received much attention due to their advantageous properties, such as low density, high mechanical strength, high thermal conductivity and low coefficient of thermal expansion (Inakagi et al., 2015; Gul and Yardim, 2015). Carbon foams are cellular structures that consist of randomly distributed pores with typical sizes between 100 and 500 μm. These unique properties, which mainly depend on the precursors' features and synthesis conditions, make carbon foams high performance engineering materials, and determine their many potential applications in numerous industries. Carbon foams can be produced as materials with thermal insulating properties, and could be applied as construction materials for airplanes, rockets and thermal management systems (Gallego et al., 2003; Klett et al., 2000). Carbon foams are promising radar absorbers, however these materials can be manufactured also with desired electrical resistance, dielectric constant and radar reflection coefficient, suitable for advanced radar antenna construction (Fang et al., 2007; Yang et al., 2004). Carbon foams are relatively inert and stable even at high temperatures and radiation – they are suitable for nuclear shields and rods for nuclear reactors (Gallego et al., 2006). The inertness and mechanical strength of carbon foams determine the suitability of these materials for bone surgery materials, prosthetics and tooth implants (Mathieu et al., 2006).

Ford firstly prepared carbon foams by the pyrolysis of thermosetting polymer in 1964 (Ford, 1964). From there on, carbon foams were successfully produced by using coal, polyimide, melamine, resorcinol/formaldehyde, biomass materials like cork and olive stones, as well as from mesophase pitches as alternative precursors (Inakagi et al., 2015; Gul and Yardim, 2015; Kim et al., 2015; Nagel et al., 2014; Szeluga et al., 2015).

The effect of the precursor on the structure and properties of the obtained carbon foams is of great significance and it is under vast investigations (Klett et al., 2000). When

coal-derived pitches are used as precursors, a preliminary treatment is usually required before the foaming process, in order to adjust the viscosity and plastic properties of the pitch that would allow an effective foaming process (Duk et al., 1986; Petrova et al., 2005). Recently, a relatively simple and low cost method was developed for making mesophase-pitch-based carbon foams at low pressure and fast heating rate during the foaming process without a stabilization treatment (Tsyntsarski et al., 2010). Carbon foams with an anisotropic texture and high mechanical strength were produced using precursors obtained after thermo-oxidation treatment of commercial coal-tar pitch with mineral acids (Tsyntsarski et al., 2010). These carbon foams exhibit outstanding mechanical properties as well as a good performance as catalysts supports (Tsyntsarski et al., 2010; Velasco et al., 2010).

The microstructure of carbon foam materials is of key interest, since it determines their functional performances. Thus, a comprehensive characterization of the physical and chemical properties of carbon foams is required in order to obtain information on structure-property relationships. The goal of this work is to yield new insights into the micro- and nanoscale properties of carbon foams derived from commercial coal-tar pitch precursors treated with H_2SO_4 and HNO_3 and finally annealed at 1000 ºC and 2000 ºC. Herein, we report on the investigation of the latter carbon foams with emphasis on the correlation of morphological and electronic properties using scanning electron microscopy (SEM), transmission electron microscopy (TEM), atomic force microscopy (AFM), X-ray photoelectron spectroscopy (XPS) and micro-spot near-edge X-ray absorption fine structure (μ-NEXAFS) spectroscopy. The obtained microstructural information is important for tailoring the properties of the coal-tar pitch precursor in order to achieve high performance carbon foam materials.

Materials and methods

The preparation of foaming precursors has been explained in details elsewhere (Tsyntsarski et al., 2010). In summary, the thermo-oxidation treatment of commercial coal-tar pitch with H_2SO_4 and HNO_3 was conducted at 120 ºC with continuous stirring. The modified samples were heated up to 350 ºC at atmospheric pressure and after that up to 580 ºC in a N_2 atmosphere, at pressure up to 1 MPa. The resultant "green" foams were calcinated at 1000 ºC in N_2 atmosphere to increase the strength and further evolving of volatiles. Finally, the resultant foams were heated consecutively first at 1000 ºC for 1 h and then at 2000 ºC in Ar atmosphere. The carbon foams (CFPs) prepared from precursors treated with H_2SO_4 are denoted as CFPST, while the samples prepared from precursors treated with HNO_3 are denoted as CFPNT, where T indicates the final heating temperature (1000 ºC or 2000 ºC).

The morphology and the microstructure of the CFPs were analyzed by SEM (JEOL 5510) applying gold coating before the observation. The TEM investigations were performed on a JEOL 2100 scanning transmission electron microscope. The XPS studies were carried out on an ESCALAB MK II (VG Scientific) system with base pressure of 1.10^{-8} mbar. The XPS spectra were taken using an unmonochromatized Mg Kα source (hν=1256.6 eV) with the sample surface positioned normal to the detector. For carbon materials, this geometry provides XPS sampling depth of ~10 nm (McArthur et al., 2014). The C1s spectra have been fitted into spectral components using Lorentzian line shapes convoluted with a major Gaussian contribution as model functions.

Micro-spot near-edge X-ray absorption fine structure (μ-NEXAFS) spectroscopy and X-ray imaging were performed using the PolLux scanning transmission X-ray microscope (STXM) at the Swiss Light Source (SLS) (Raabe et al., 2008). For specimen preparation, CFP microparticles were deposited onto a Si_3N_4 window (Silson Ltd., Northampton, UK) of 100 nm thickness. The STXM chamber was turbo-pumped and the samples were imaged in

transmission mode at about $5x10^{-6}$ mbar. The X-ray beam was focused with a Fresnel zone plate onto the sample and the transmitted photon flux was measured using a photomultiplier tube (Hamamatsu 647P) mounted behind the specimen, along the axis of the incident beam. Therefore, the technique is considered to be mostly bulk-sensitive. The diffraction limited spot size at the sample is determined by the width of the outermost zone of the zone plate, ~40 nm for the PolLux STXM experiments (Huthwelker et al., 2010). The PolLux STXM uses linearly polarized X-rays from a bending magnet in the photon energy range between 200 eV and 1200 eV. Carbon *K*-edge μ-NEXAFS spectra were collected in line mode, i.e., the transmitted signal was recorded while a line trajectory was scanned across the center of a particle at each value of the photon energy through the spectrum. The average spectra presented were calculated from 5 different foam microparticles spectra.

Experiments on the dispersal of CFPN1000 sample in dilute ethanol (96 vol. %, Sigma-Aldrich) suspension were conducted using a standard ultrasonic water bath at room temperature. The suspension was continuously ultrasonicated at 45 kHz for 5 min. SEM and AFM images were obtained from the resulting suspension drop-cast on a glass substrate. TEM was done by drop casting the dispersed solution directly onto a copper TEM-grid. AFM imaging was performed on the NanoScopeV system (Bruker Inc.) operating in tapping mode in air at room temperature. Silicon cantilevers (Tap 300 Al-G, Budget Sensors, Innovative solutions Ltd, Bulgaria) with cantilever spring constant in the range of 1.5–15 N/m and the resonance frequency 150±75 kHz were used. The tip radius was less than 10 nm. The scan rate was set at 0.5 Hz and the images were captured in height modes with 512×512 pixels in a JPEG format. Subsequently, all the images were flattened by means of the Nanoscope software.

Compressive strength measurements were performed using TA Instruments DMA 2980 Dynamic Mechanical Analyzer. The measurements were carried out at constant

frequency (1 Hz) and isothermal temperature holds (20 ºC). Cylindrical samples having a diameter about 25 mm and height about 30 mm were placed between parallel plates of small compression clamp.

Results and discussion

Fig. 1 describes the morphology of CFPS and CFPN samples. As shown, the carbon foams are characterized by a reticular vitreous structure with foam cells of size in the range of 200-350 μm. The presence of cracks in the matrices of all materials is also observed, characteristic for well-developed CFP structure. The X-ray diffraction (XRD) analysis of the materials revealed that the CFPs are partially graphitic with interlayer distances between the graphitic carbon sheets ranging from 0.3469 nm for CFPS1000 to 0.3424 nm for CFPN2000 (Tsyntsarski et al., 2010). The degree of graphitization follows an order of CFPN2000>CFPS2000>CFPN1000>CFPS1000 and it has been concluded that by using nitric acid as modifying agent more ordered foam structure can be obtained.

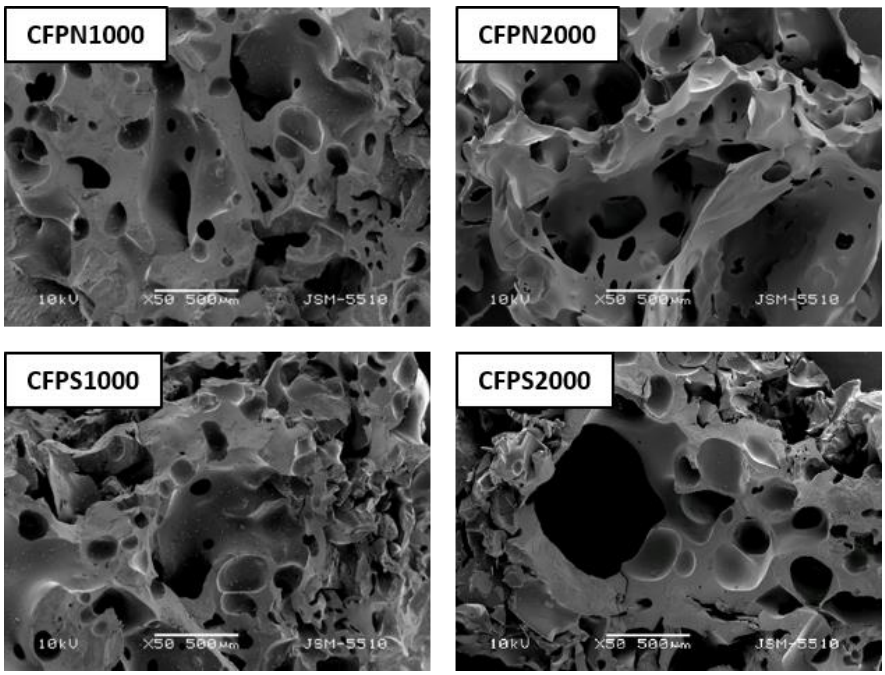

Fig. 1. SEM images of CFPN and CFPS foams.

The high-magnification SEM images (Fig. 2) of the CFPs demonstrate complex microstructural features. In case of CFPN1000, many microspheres are observed on the surface of the sample. As seen, these microspheres either sit in the pits or lie near to the pits in the carbon matrix. The SEM close-up view of CFNP1000, shown as an insert in Fig. 2a, reveals the presence of larger agglomerates of closely-packed microspheres. Furthermore, an evident clearance between the microspheres and the CFP surface can be detected which implies that the particles are not firmly-anchored to the matrix. Additionally, a large number of pits with round geometry etch the sample surface. SEM-derived histograms of the microsphere and pit size distributions are shown in Fig. 2c,d. The statistical analysis yields microspheres and pits with average diameters of 0.28±0.01 μm and 0.31±0.02 μm, respectively.

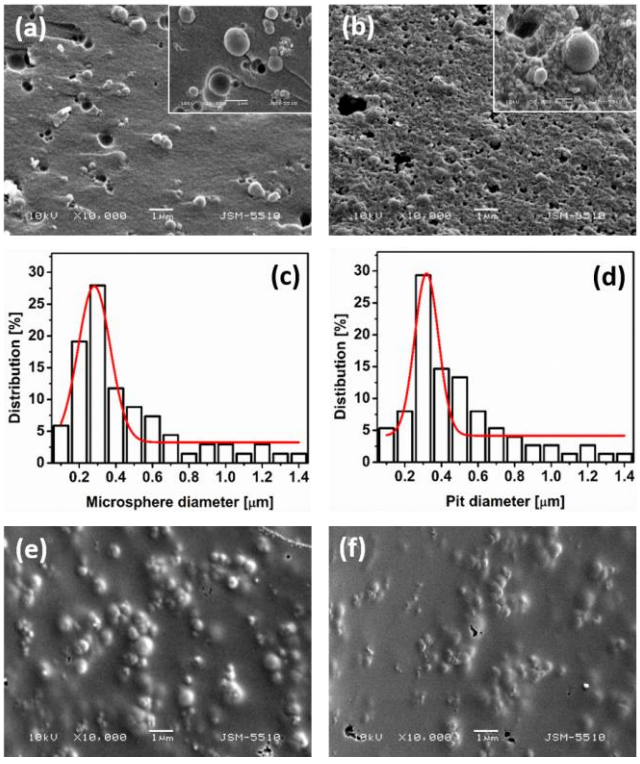

Fig. 2. High-magnification SEM images of (a) CFPN1000, (b) CFPS1000, (e) CFPN2000 and (f) CFPS2000. In the insert of (a) the micron bar length is 1 μm. In the insert of (b) the micron bar length is 0.5 μm. Histograms of (c) microsphere and (d) pit size distributions for CFPN1000.

Apparently, the pit diameter is only slightly larger than the microspheres and on the basis of our SEM observations one can conclude that the pits are the places of origin of the microspheres. Thus, we presume that the microstructure of CFPN1000 is composed of microspheres embedded in the carbon foam matrix. The origin of microspheres could be ascribed to species formed during foaming process, as a result of formation of pores accompanied by evolving of volatiles or degradation processes, e.g. cleavage of hydrocarbon chains. The high-magnification SEM image of CFPS1000 (see Fig. 2b) reveals the presence of microspheres as well, but in contrast to the CFPN1000, they are completely incorporated into the porous structure of CFP. The SEM close-up view of CFPS1000 (see the insert in Fig. 2b) indicates the presence of only a few microspheres standing on the surface of the sample. Remarkably, our SEM inspections of many different surface regions of CFPN1000 and CFPS1000 confirmed the morphological differences between these two samples observed in Fig. 2a,b. It is reasonable to assume that the microstructural differences between CFPN1000 and CFPS1000 are related to the differences in the chemical composition of the precursors. As reported before, thermo-oxidation of coal tar pitch with H_2SO_4 and HNO_3 leads to the formation of condensed aromatic structures as a result of polycondensation reactions of the formed oxygen containing compounds and polymerization reactions of double bond containing substances (Petrova et al., 2005). Solubility tests performed to obtain information for the chemical composition of parent and modified pitches have shown considerable differences, depending on the reagent (H_2SO_4 and HNO_3). For instance, H_2SO_4 treated pitch contains greater number of condensed aromatic structures (Tsyntsarski et al., 2010). The high-magnification SEM images of CFPS2000 and CFPN2000 are shown in Fig. 2e,f. Evidently, the microspheres observed in the micrographs of low-temperature treated CFPs are firmly buried in the graphitized matrix of CFPS2000 and CFPN2000 foams. Moreover, the pits and pores are no longer detected and only a few irregularly shaped holes are noticeable in both

images. These temperature-dependent morphology changes can be ascribed to strong bonding between microspheres and CFP matrix at 2000 °C. The thermodynamic driving force behind this phenomenon is the quest for a reduction of the surface free energy of the microspheres. Besides, the enhanced graphitization at 2000 °C leads to more efficient alignment of the graphene sheets and subsequently better compaction and increased density of the CFP walls.

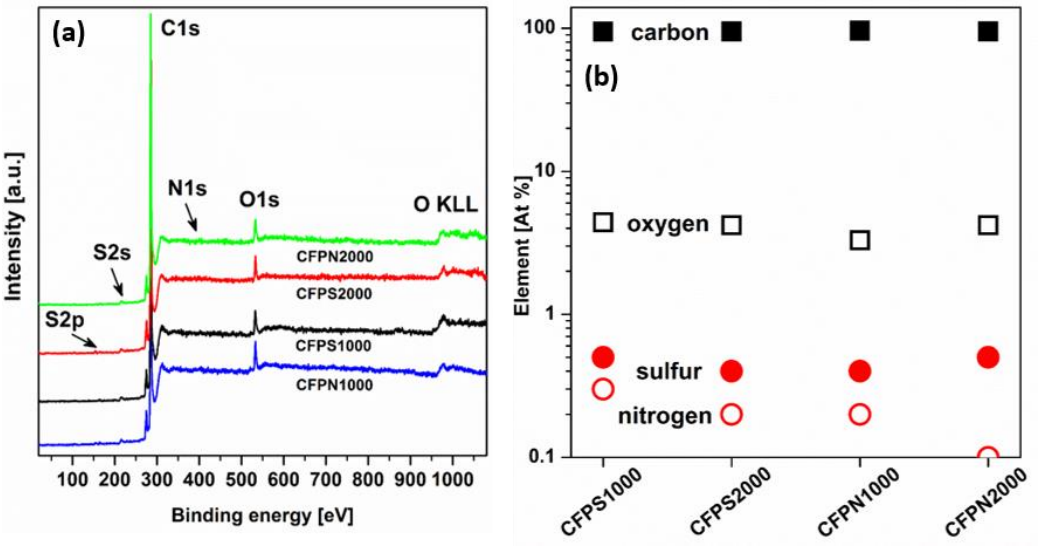

Fig. 3. (a) XPS survey spectra of CFPN and CFPS samples and (b) the corresponding C, O, N and S atomic concentrations.

The surface characteristics of CFPN and CFPS samples have been assessed *via* XPS. Fig. 3a compares the survey spectra of the CFPs and, as shown, the spectra of all samples consist of intense carbon (at ~285 eV) and oxygen (at ~532 eV) peaks. A closer inspection of the XPS survey spectra reveals weak contributions assigned to nitrogen and sulfur as well. The corresponding XPS-derived elemental atomic concentrations are summarized in Fig. 3b. The high-resolution O1s, S2p and N1s XPS spectra of the CFPs are compared in Fig. 4. The formation of oxygen containing structures in CFPs is a result of the thermo-oxidation treatment. The deconvolution procedure shows the presence of several chemistries of oxygen, including one at ~531.2 eV due to C=O bonds, one at ~532.6 eV due to C-O bonds and one at

~535.6 eV, corresponding to chemisorbed oxygen and adsorbed water (see Fig. 4a). As shown, the O1s spectra of the high-temperature treated samples contain a small component at ~530 eV, which may be attributed to conjugated carbonyl, such as quinone groups (Parent et al., 2016). The S2p core level spectra of CFPs (Fig. 4b) exhibit a doublet at 163.9 and 165.1 eV, which can be ascribed to -C-S-C- sulphide bridges (Valle-Vigón et al., 2013). Very low intensity signals centered at ~401.2 eV are observed in the N1s envelope of the samples (Fig. 4c). This signals can be assigned to quaternary nitrogen, also called ‘‘graphitic nitrogen’’, in which nitrogen atoms are incorporated into the graphene layers (Shao et al., 2010).

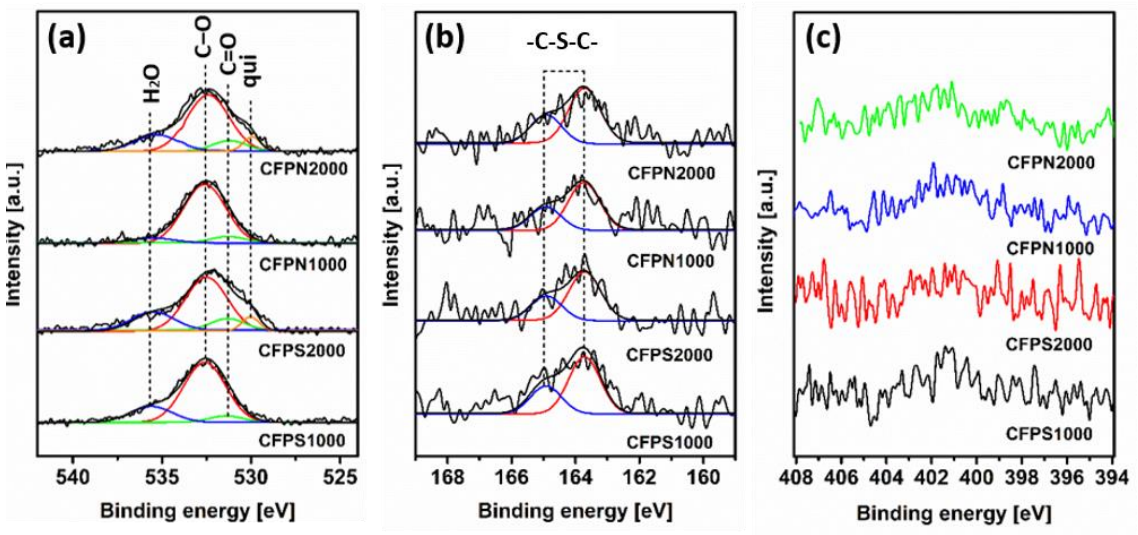

Fig. 4. (a) O1s, (b) S2p and (c) N1s high-resolution XPS spectra of CFPN and CFPS samples.

Regarding the sulfur and nitrogen content and their bonding environments, there are some important aspects that should be considered. First, according to the XPS-derived elemental atomic concentrations (see Fig. 3b) the nitrogen and sulfur content cannot be correlated with the acid (nitric or sulfuric) applied for pitch treatment. More specifically, CFPN2000 sample contains the largest amount of sulfur while the nitrogen content is almost

negligible. Second, the XPS data suggest that these heteroatoms are covalently incorporated into carbonaceous samples. Coal tar is a very complex material, consisting of a variety of compounds of different functionality and a wide range of molecular weight. The dominant compounds are aromatic hydrocarbons with one to eight rings, but homologous heterocyclic compounds containing oxygen, nitrogen and sulfur are also present in small amount (Li and Suzuki, 2010). The elemental analysis of the coal-tar pitch utilized in the present study revealed sulfur and nitrogen content of 0.5 and 0.9 wt.%, respectively (Tsyntsarski et al., 2010). Thus, we presume that the presence of these elements in the CFPs is mainly due to the decomposition and reactions of the heterocyclic compounds during thermo-oxidation and carbonization/graphitization steps.

The high-resolution C1s XPS spectra of the CFPs are compared in Fig. 5. For CFPS2000 and CFPN2000, XPS spectra look very similar and in both cases the deconvolution of the C1s regions is achieved with five components centered at 284.5, 285.1, 286.2, 288.3, and 290.5 eV. The main peak at 284.5 eV originates from a graphite signal (sp^2 carbon) (Girard-Lauriault et al., 2012). The peak at 285.1 eV is attributed to sp^3 carbon (Rybachuk and Bell, 2009). The peaks at 286.2 eV and 288.3 eV are typical of carbon atoms bound to one oxygen atom with a single bond (alcohol, ether) and to carbonyl groups, respectively (Beamson and Briggs, 1992). A peak attributed to π–π^* shake-up bonds is observed at 290.5 eV (Girard-Lauriault et al., 2012). The sp^2/sp^3 ratios calculated from the XPS spectra are 5.6 and 4.9 for CFPN2000 and CFPS2000, respectively. These values indicate the extent of graphitization and are in agreement with the XRD-derived degree of ordering of the samples (see above).

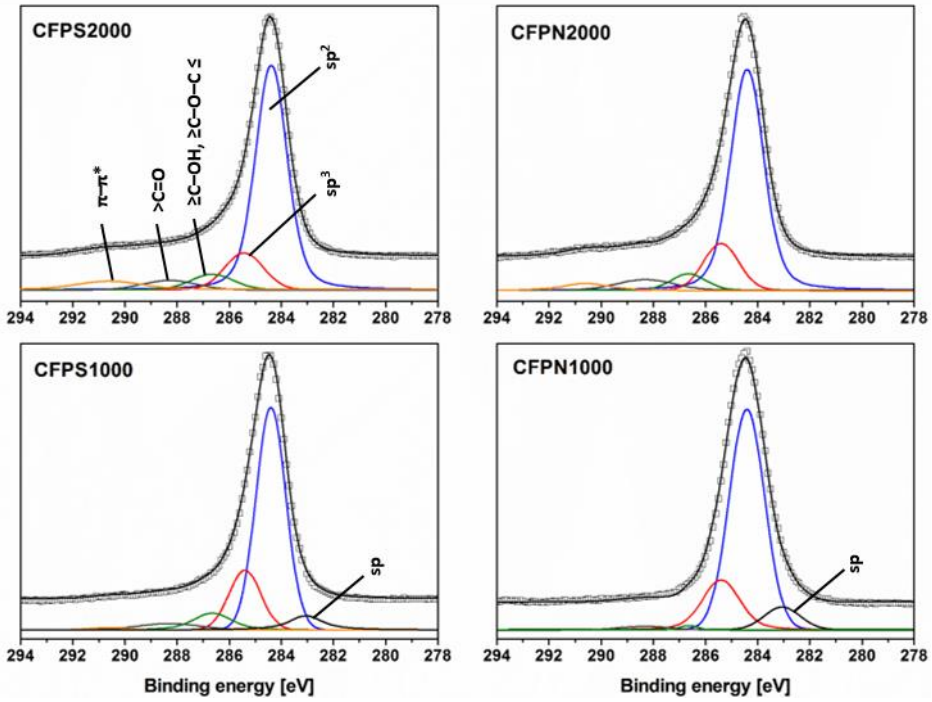

Fig. 5. High-resolution C1s XPS spectra of CFPN and CFPS samples. The open symbols and solid lines represent the raw experimental data and the results of peak fitting, respectively.

Evidently, CFPS1000 and CFPN1000 C1s photoemission spectra (see Fig. 5) demonstrate decreased photoemission intensity at high-binding energies in comparison to CFSP2000 and CFPN2000. The observed spectral variation indicates a difference between the electronic state of carbon atoms in the low- and high-temperature treated samples. In contrast to the high-temperature treated CFPs, the curve fitting analysis of the CFPS1000 and CFPN1000 XPS spectra reveals a signal at 283.2 eV. The binding energy reported for the latter peak corresponds to those usually found in XPS measurements with carbides (Beamson and Briggs, 1992). However, since no carbide-related elements have been detected in the survey XPS spectra, this interpretation should be ruled out. Weckhuysen et al. (1998) reported that during the conversion of methane to benzene over a Mo/H-ZSM-5 catalyst at 700 ºC, a hydrogen-poor sp-type or pregraphitic-type of carbon with a C1s binding energy of 283.2 eV is formed. Furthermore, Rybachuk and Bell (2009) observed sp-hybridised species at ~283 eV

binding energy in the XPS spectrum of amorphous hydrogenated carbon sample. In accordance with the above mentioned reports we attribute the low binding energy component (283.2 eV) in CFPS1000 and CFPN1000 C1s XPS spectra to sp-bonded carbon species. Thus, the photoemission results suggest that three different types of carbon (sp-, sp^2- and sp^3-hybridised) are present in the low-temperature treated CFPs. The percentage of sp-, sp^2- and sp^3-bonded species was calculated on the basis of integrating peak areas for the three respective line-functions and was found to be 7.6% sp, 73.8% sp^2 and 18.6% sp^3 for CFPN1000 and 6.7% sp, 72.3% sp^2 and 21.0% sp^3 for CFPS1000.

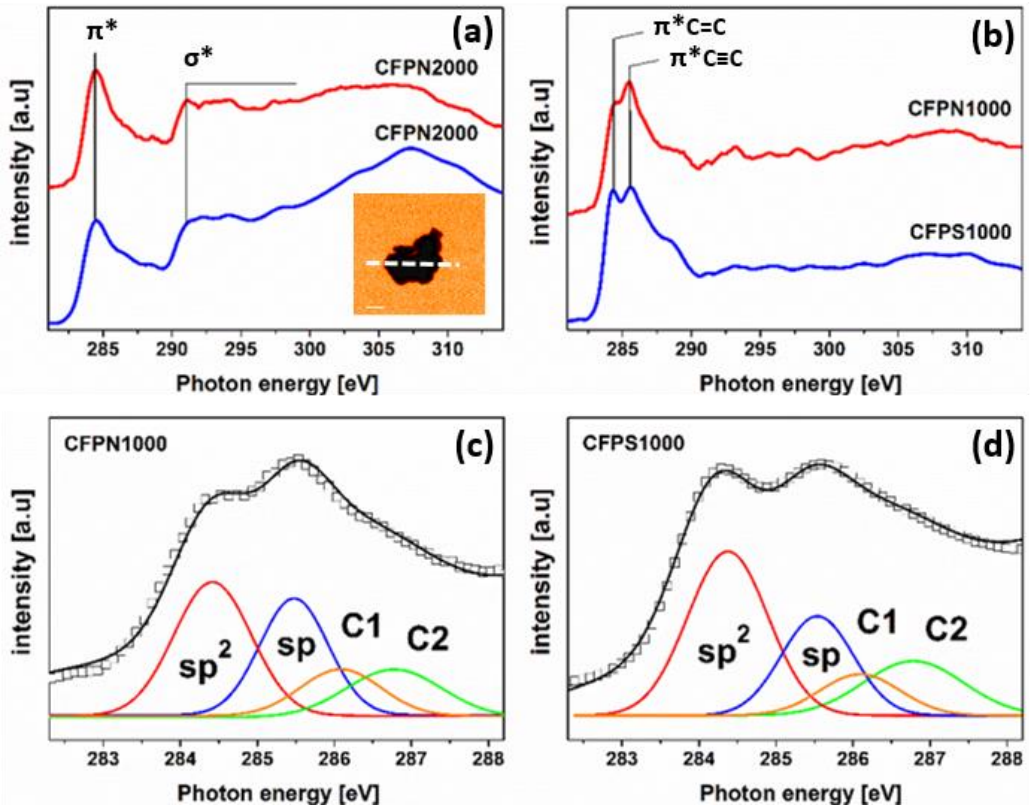

Fig. 6. (a) C *K*-edge μ-NEXAFS spectra of CFPN2000 and CFPS2000 samples. The dashed line indicates the position of the μ-NEXAFS linescan across a carbon foam microparticle (insert); the micron bar length in the STXM image is 5 μm. (b) C *K*-edge μ-NEXAFS spectra of CFPN1000 and CFPS1000 samples. (c,d) Deconvolution of the 282-288 eV region of CFPN1000 and CFPS1000 spectra. The open symbols and solid lines represent the raw experimental data and the results of peak fitting, respectively.

In order to gain insight into the bulk chemical structure of the CFPs, STXM measurements have been performed. STXM technique provides both high chemical sensitivity *via* μ-NEXAFS with a spectral resolving power E/ΔE>5000 at the N *K*-edge and X-ray imaging with a spatial resolution less than 40 nm (Raabe et al., 2008). The X-ray transmission image of a representative CFP microparticle taken at 300 eV photon energy is shown as an insert in Fig. 6. The dashed line across the particle indicates the position of the μ-NEXAFS line scan. The local carbon *K*-edge NEXAFS spectra obtained from the CFPS and CFPN particles are compared in Fig. 6a,b. The NEXAFS line scans obtained from different regions of a single particle have shown identical resonance intensities, i.e. the samples are chemically homogenous, constituted of randomly oriented graphitic regions. The spectra of high-temperature treated samples show two main features near 284.5 eV and 291.1 eV, which are assigned to the unoccupied π* and σ* states, respectively (Batson, 1993). The π* feature at 284.5 eV is the characteristic of the sp^2 C=C bond (Morar et al., 1985), while the feature at 291.1 eV shows the sp^2-derived unoccupied σ* bands (Ma et al., 1992). Overall, the line shapes of these two spectra are typical for the graphitized carbon materials (Batson, 1993). The relatively broad σ* resonance and the absence of a sharp excitonic resonance just below the σ* feature indicate that the sp^2 network in CFPS2000 and CFPN2000 is substantially defective. The μ-NEXAFS spectra of the low temperature treated samples (see Fig. 6b) show a strong decrease of the σ* feature at ~291.1 eV in comparison to the spectra of the high-temperature treated samples which is due to the lower degree of graphitization and the presence of various in-plane defects in the graphitic layers in the low-temperature treated samples. Interestingly, the spectra of CFPS1000 and CFPN1000 show an additional strong π* resonance at ~285.5 eV. In the C *K*-edge NEXAFS spectra of C_2H_2 and C_2H_4, the simplest organic molecules with sp and sp^2 bonds, resonances occur at ~286 eV (excitation into $\pi^*_{C\equiv C}$) and at ~285 eV eV (excitation into $\pi^*_{C=C}$) (Stöhr, 1992). Furthermore, Ravagnan et al. (2011)

reported that in the NEXAFS spectra of free carbon nanoparticles the π* resonances from sp and sp^2-bonded carbon atoms are located at 285.9 eV and at 284.7 eV, respectively. Thus, based on these results, we attribute the π* resonances at ~285.5 eV in the μ-NEXAFS spectra of CFPS1000 and CFPN1000 to the presence of sp-hybridised carbon species. In order to evaluate in more detail the π* contributions in the NEXAFS spectra of CFPS1000 and CFPN1000, the peaks in the 282-288 eV range were fitted to Gaussian functions, as shown in Fig. 6c,d. Along with the components assigned to sp and sp^2 hybrids, additional transitions at 286.1 eV and 286.8 eV (labeled as C1 and C2) were also resolved. The C1 component corresponds to π* resonances in species containing aliphatic carbon, while ketone C=O, carbonyl-substituted aromatic carbon and phenolic C-OH can all have π* resonances at 286.8 eV (Di Stasio and Braun, 2006; Tivanski et al., 2007). This result is in accordance with the XPS observations (see above). The area of each fitted peak provides a good estimate of the relative contribution of different species to the π* intensities of the samples. The integrated intensity ratios of the sp^2 and sp π* components ($\pi^*_{C=C/}$ $\pi^*_{C\equiv C}$) is 1.3 for CFPN1000 and 1.9 for CFPS1000. A direct interpretation of this result is that CFPN1000 has a higher concentration of sp-bonded carbon atoms compared to the CFPS1000. Also, the comparison of XPS and NEXAFS spectra of the low-temperature treated CFPs reveals that the concentration of sp-hybridised species at the surface regions of the samples (assessed *via* XPS) is substantially lower than the concentration detected in the bulk of the materials (assessed *via* STXM-NEXAFS). We presume that this is due to the fact that the sp carbon chains present on the sample surfaces convert to sp^2 structures when the samples are exposed to air.

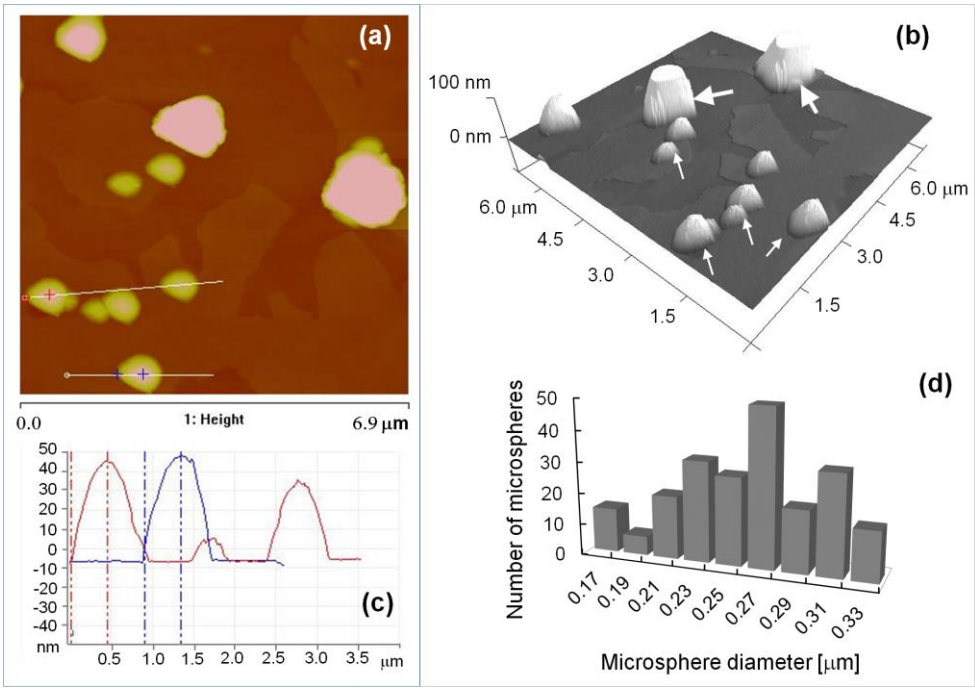

Fig. 7. AFM images of ultrasonicated CFPN1000 suspension drop-cast on a glass substrate. AFM images in (a) 2D format and (b) 3D format (small arrows point to the individual microspheres, while the big arrows are directed to the larger agglomerates of closely-packed microspheres). The scanned area was 7×7 µm with z-scale 100 nm. (c) Cross section performed across individual microspheres. (d) Histogram of the size distribution of the microspheres.

In the course of our microscopy studies of the CFPs it was found that the microspheres observed in Fig. 2a are poorly bound to the surface of the samples and could easily be removed. We succeeded to remove part of the microspheres from CFPN1000 powders by applying gentle ultrasonication of their ethanol suspension. AFM images in 2D and 3D format obtained from the ultrasonicated suspension drop-cast on a glass substrate are depicted in Fig. 7a,b. On the images the well-defined microspheres, randomly attached to the glass surface, are evident. From the images one can distinguish the individual microspheres (small arrows in Fig. 7b) from the larger agglomerates of closely-packed microspheres (big arrows in Fig. 7b). The corresponding height profiles taken in the direction of the lines are shown in Fig. 7c. In dynamic (tapping) AFM mode because of the nature of attractive forces, the tip might

contribute to height gain or loss (Lai et al., 2015) and, therefore, for more accurate analysis of the diameter of microspheres we adopted the AFM volumetric method (Fuentes-Perez et al., 2013) as mages from three independent experiments were analyzed. The analysis of the AFM data (see Fig. 7d) shows the presence of microspheres with an average diameter of 0.24±0.02 μm. Remarkably, the latter value is very close to the SEM-derived average diameter of microspheres (0.28±0.01 μm, see above).

The SEM image obtained from the ultrasonicated suspension drop-cast on a glass substrate is depicted in Fig. 8a. Again, many microspheres ranging in diameter from <1 μm to 2.5 μm are detected. Besides, several irregularly shaped particles from the CFP matrix are also observed. In contrast to the pristine CFPN1000 sample, the SEM image (the insert of Fig. 8a) of the ultrasonicated and additionally rinsed with ethanol CFP particles shows only empty pits on the surface of the sample. The latter "microsphere-free" sample was subjected to XPS analysis and the resulting C1s photoemission spectrum is compared with the spectrum of the pristine CFPN1000 foam in Fig. 8b. Evidently, the relative intensity of the shoulder at ~283 eV (marked with arrow) ascribed to the sp-type of carbon, decreases after ultrasonication of the material. In order to emphasize the alteration, XPS difference spectrum (pristine CFPN1000-minus-ultrasonicated CFPN1000) is presented as an insert of Fig. 8b. As one can see, a prominent peak centered at 283.2 eV appears in the difference spectrum. This result unambiguously suggests that the microspheres (see Figs. 2a, 7a and 8a) are largely responsible for the latter photoemission signal. That is, the microspheres are essentially made of sp-hybridised carbon chains. To further probe microspheres internal structure, TEM analysis of the suspension drop-cast on a TEM-grid was performed. Fig. 8c shows a bunch of four microspheres attached to a larger particle resulting from the foam matrix. The high-resolution TEM examination, as shown in Fig. 8d, reveals the amorphous structure of the microspheres.

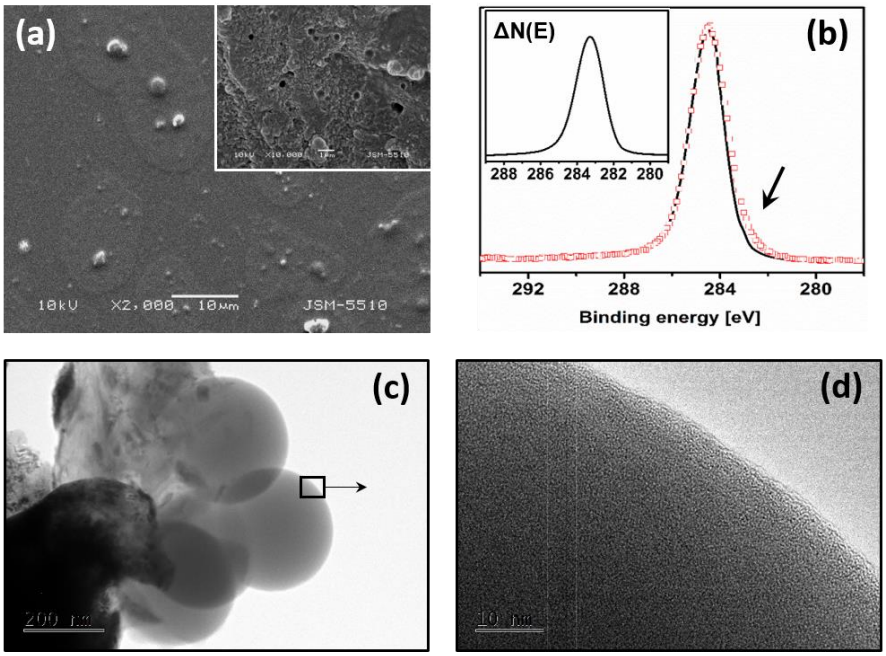

Fig. 8. (a) SEM image of ultrasonicated CFPN1000 suspension drop-cast on a glass substrate. The insert shows the SEM image of the ultrasonicated CFPN1000 sample; the micron bar length is 1 μm. (b) High-resolution C1s XPS spectra of the pristine (open symbols) and ultrasonicated (solid line) CFPN1000 samples. The insert shows the corresponding XPS difference spectrum. (c) TEM top view image of microspheres resulting from CFPN1000. (d) HRTEM image of the edge of a microsphere.

The data presented above indicate that at temperatures between 1000 ºC and 2000 ºC there is an alternative pathway for the formation of graphite containing microspheres. Namely, the formation of the graphitized sp^2-sp^3 matrix of the carbon foams involves mainly polycyclic aromatic structures resulting from the modification and foaming processes. Instead, the sp rich microspheres transform into graphite at temperatures >1000 ºC in a non-aromatic pathway. We presume that the microspheres contain chains of $–(C{\equiv}C)_n–$ type that serve as additional precursor in the formation of graphite. Also, the concentration of the sp rich microspheres is enhanced in the bulk of the low-temperature treated CFPs, as inferred from the differences between the NEXAFS and XPS signals. To the best of our knowledge, the formation of such microstructures during the foaming of coal-tar pitches has not been

reported before. The XPS and NEXAFS analyses reveal that the use of nitric acid in the thermo-oxidation step favors the formation of the latter species. Moreover, in the case of CFPN1000 the microspheres could easily be detached from the dense carbon foam matrix, while for CFPS1000 the microspheres are firmly implanted in the porous framework. This could be explained by the increased content of quinoline insoluble and toluene insoluble fractions (Tsyntsarski et al., 2010) in the pitch precursor for CFPS1000, which is due to favored polycondensation and polymerization reactions that run during the pre-treatment with H_2SO_4.

As shown in Fig. 2a,b, CFPN1000 foam cell walls are dense while CFPS1000 walls possess a porous microstructure. These results are in accordance with the previously reported relative densities of CFPN and CFPS samples. That is, the relative density varies between 0.52 g/cm^3 to 0.59 g/cm^3 and follows an order of CFPN2000>CFPS2000>CFPN1000>CFPS1000 (Tsyntsarski et al., 2010). Interestingly, the relative density of the low-temperature treated CFPs increases with the increasing concentration of sp-bonded carbon atoms in the samples as indicated by XPS and NEXAFS data. For CFPN2000 and CFPS2000, the relative density variations can be associated with the enhanced non-aromatic graphitization of CFPN1000. Thus, despite of the similar SEM micrographs of the high-temperature treated CFPs (see Fig. 2e,f), their properties reflect a "memory" of the initial thermo-oxidation processes that extends up to 2000 °C. It is well known that high relative density implies presence of thicker cell walls and shorter cell edges, which promote higher compressive strength (Gallego et al., 2003). The compressive strength measurements of CFPN and CFPS are compared in Fig. 9. Apparently, the compressive strength increases with the relative density and it can be seen that the highest values are obtained for CFPN1000 and CFPN2000 samples, respectively. Thus, our microscopy and spectroscopy observations reveal that the temperature-induced microstructural

transformations of the CFPs depend on the reagent (nitric *vs.* sulfuric acid) used for pitch treatment and should be controlled by using appropriate processing conditions in order to obtain carbon foam materials with the desirable physical properties.

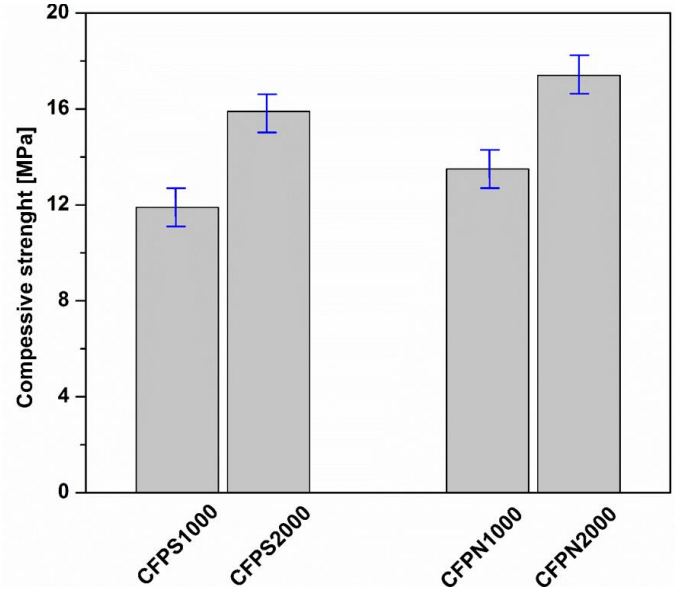

Fig. 9. Histograms of the compressive strength of CFPN and CFPS samples.

Conclusions

The following conclusions can be drawn from our combined microscopy and spectroscopy survey. First, the microscopy observations revealed that the thermo-oxidation modification of coal-tar pitch and subsequent foaming procedure and heating at 1000 ºC lead to the formation of amorphous carbonaceous microspheres embedded in the partially graphitized carbon foam matrix. These microspheres are mainly composed of sp-bonded species and, furthermore, their presence depends on the modifier (higher concentration of sp-bonded carbons in the foam derived from the precursor treated with HNO_3). Second, at temperatures above 1000 ºC the microspheres experience chemical transformations in a non-aromatic pathway and at 2000 ºC they are spectroscopically identical with the bulk material (sp^2-sp^3 matrix). The SEM analysis provides an evidence that at 2000 ºC both CFPs exhibit

similar microstructure consisting of many spherical structures, submerged into the dense carbon matrix. The compressive strength of the carbon foams increases with the increasing concentration of sp-bonded carbon atoms in the low-temperature treated samples. The presented microstructural findings are of importance for further improvement of the effect of the precursor on the structure and properties of carbon foams.

Acknowledgements

The work was done under the frame of MPNS COST Action MP 1306. The PolLux end station was financed by the German Minister für Bildung und Forschung (BMBF) through contracts 05KS4WE1/6 and 05KS7WE1.

References

Batson, P.E., 1993. Carbon 1s near-edge-absorption fine structure in graphite. Phys. Rev. B 48, 2608-2610.

Beamson, G., Briggs, D., 1992. High Resolution XPS of Organic Polymers: Scienta300 Database. John Wiley and Sons, Chichester.

Di Stasio, F., Braun, A., 2006. Comparative NEXAFS Study on Soot Obtained from an Ethylene/Air Flame, a Diesel Engine, and Graphite. Energy & Fuels 20, 187-194.

Duk, P.Y., Korai, Y., Mochida, I., 1986. Preparation of anisotropic mesophase pitch by carbonization under vacuum. J. Mater. Sci. 21, 424-428.

Fang, Zh., Li, Ch., Sun, J., Zhang, H., Zhang, J., 2007. The electromagnetic characteristics of carbon foams. Carbon 45, 2873-2879.

Ford, W., 1964. Method of making cellular refractory thermal insulating material. US patent 3121050.

Fuentes-Perez, M.E., Dillingham, M.S., Moreno-Herrero, F., 2013. AFM volumetric methods for the characterization of proteins and nucleic acids. Methods 60, 113-121.

Gallego, N.C., Burchell, T.D., Klett, J.W., 2006. Irradiation effects on graphite foam. Carbon 44, 618-628.

Gallego, N.C., Klett, J.W., 2003. Carbon foams for thermal management. Carbon 41, 1461-1466.

Girard-Lauriault, P.L., Illgen, R., Ruiz, J.C., Wertheimer, M.R., Unger, W.E.S., 2012. Surface functionalization of graphite and carbon nanotubes by vacuum-ultraviolet photochemical reactions. Appl. Surf. Sci. 258, 8448-8454.

Gul, A., Yardim, F., 2015. Preparation and characterization of mesophase pitch based carbon foam produced at low pressure. J. Por. Mater. 222, 851-857.

Huthwelker, T., Zelenay, V., Birrer, M., Krepelova, A., Raabe, J., Tzvetkov, G., Vernooij, M.G.C., Ammann, M., 2010. An in situ cell to study phase transitions in individual aerosol particles on a substrate using scanning transmission x-ray microspectroscopy. Rev. Sci. Instr. 81, 113706.

Inagaki, M., Qiu, J., Guo, Q., 2015. Carbon foam: Preparation and application. Carbon 87, 128-152.

Kim, J.H., Jeong, E., Lee, Y.S., 2015. Preparation and characterization of graphite foams. J. Ind. Eng. Chem. 32, 21-33.

Klett, J., Hardy, R., Romine, E., Walls, C., Burchell, T., 2000. High thermal-conductivity, mesophase-pitch-derived carbon foams: effect of precursor on structure and properties. Carbon 38, 953-973.

Lai, C.-Y., Santos, S., Chiesa, M., 2015. General interpretation and theory of apparent height in dynamic atomic force microscopy. RSC Advances, 5 (97), 80069-80075.

Li, C., Suzuki K., 2010. Resources, properties and utilization of tar. Resour. Conserv. Recy. 54, 905-915.

Ma, Y., Wassdahl, N., Skytt, P., Guo, J., Nordgren, J., Johnson, P.D., Rubensson, J.E., Boske, T., Eberhardt, W., Kevan, S.D., 1992. Soft X-ray resonant inelastic scattering at the C K-edge of diamond. Phys. Rev. Lett. 69, 2598-25601.

Mathieu, L.M., Mueller, T.L., Bourban, P.E., Piolettic, D.P., Muller, R., Manson, J.A.E., 2006. Architecture and properties of anisotropic polymer composite scaffolds for bone tissue engineering. Biomaterials 27, 905-916.

McArthur, S.L., Mishra, G., Easton, C.D., 2014. Applications of XPS in biology and biointerface analysis, in: Smentkowski, V.S. (Ed.), Surface analysis and techniques in biology. Springer International Publishing, Switzerland, pp 9-36.

Morar, J.F., Himpsel, F.J., Hollinger, G., Hughes, G., Jordan, J.L., 1985. Observation of a C-1s core exciton in diamond. Phys. Rev. Lett. 54, 1960-1963.

Nagel, B., Pusz, S., Trzebicka, B., 2014. Review: tailoring the properties of macroporous carbon foams. J. Mater. Sci. 49, 1-17.

Parent, P., Laffon, C., Marhaba, I., Ferry, D., Regier, T.Z., Ortega, I.K., Chazallon, B., Carpentier, Y., Focsa, C., 2016. Nanoscale characterization of aircraft soot: A high-resolution transmission electron microscopy, Raman spectroscopy, X-ray photoelectron and near-edge X-ray absorption spectroscopy study. Carbon 101, 86-100.

Petrova, B., Budinova, T., Petrov, N., Yardim, M.F., Ekinci, E., Razvigorova, M., 2005. Effect of different oxidation treatments on the chemical structure and properties of commercial coal tar pitch. Carbon 43, 261-267.

Raabe, J., Tzvetkov, G., Flechsig, U., Böge, M., Jaggi, A., Sarafimov, B., Vernooij, M.G.C., Huthwelker, T., Ade, H., Kilcoyne, D., Tyliszczak, T., Fink, R.H., Quitmann, C., 2008.

PolLux: A new facility for soft x-ray spectromicroscopy at the Swiss Light Source. Rev. Sci. Instrum. 79, 113704.

Ravagnan, L., Mazza, T, Bongiorno, G., Devetta, M., Amati, M., Milani, P., Piseri, P., Coreno, M., Lenardi, C., Evangelista, F., Rudolf, P., 2011. sp hybridization in free carbon nanoparticles-presence and stability observed by near edge X-ray absorption fine structure spectroscopy. Chem. Comm. 47, 2952-2954.

Rybachuk, M., Bell, J.M., 2009. Electronic states of trans-polyacetylene, poly(p-phenylene vinylene) and sp-hybridised carbon species in amorphous hydrogenated carbon probed by resonant Raman scattering. Carbon 47, 2481-2490.

Shao, Y., Zhang, S., Engelhard, M.H., Li, G., Shao, G., Wang, Y., Liu, J., Aksay I.A., Lin, Y., 2010. Nitrogen-doped graphene and its electrochemical applications. J. Mater. Chem. 20, 7491-7496.

Stöhr, J., 1992. NEXAFS spectroscopy. Springer, New York.

Szeluga, U., Kumanek, B., Pusz, S., Czajkowska, S., 2015. Preparation and characterization of carbon foams by carbonization of cyanate and cyanate/epoxy resins. J. Thermal. Anal. Calorimetry 122, 271-279.

Tivanski, A.V., Hopkins, R.J., Tyliszczak, T., Gilles, M.K., 2007. Oxygenated interface on biomass burn tar balls determined by single particle scanning transmission X-ray microscopy. J. Phys. Chem. A 111, 5448-5458.

Tsyntsarski, B., Petrova, B., Budinova, T., Petrov, N., Krzesinska, M., Pusz S., Majewska, J., Tzvetkov, P., 2010. Carbon foam derived from pitches modified with mineral acids by a low pressure foaming process. Carbon 48, 3523-3530.

Velasco, L.F., Tsyntsarski, B., Petrova, B., Budinova, T., Petrova, N., Parra, J.B., Ania, C.O., 2010. Carbon foams as catalyst supports for phenol photodegradation. J. Hazard. Mater. 184, 843-848.

Valle-Vigón, P., Sevilla, M., Fuertes, A.B., 2013. Functionalization of mesostructured silica-carbon composites. Mater. Chem. Phys. 139, 281-289.

Weckhuysen, B.M., Rosynek, M.P., Lunsford, J.H., 1998. Characterization of surface carbon formed during the conversion of methane to benzene over Mo/H-ZSM-5 catalysts. Catal. Lett. 52, 31-36.

Yang, J., Shen, .Z, Hao, Z., 2004. Microwave characteristics of sandwich composites with mesophase pitch carbon foams as core. Carbon 42, 1882-1885.